


## Deflection of barium monofluoride molecules using the bichromatic force: A density-matrix simulation

A. Marsman, M. Horbatsch, and E. A. Hessels <sup>\*</sup>  
(EDM<sup>3</sup> Collaboration)

*Department of Physics and Astronomy, York University, Toronto, Ontario, Canada M3J 1P3*

 (Received 17 May 2023; accepted 30 June 2023; published 17 July 2023)

A full density-matrix simulation is performed for optical deflection of a barium monofluoride ( $^{138}\text{Ba}^{19}\text{F}$ ) beam using the bichromatic force, which employs pairs of counterpropagating laser beams that are offset in frequency. We show that the force is sufficient to separate BaF molecules from the other products generated in a helium-buffer-gas-cooled ablation source. For our simulations, the density-matrix and force equations are numerically integrated during the entire time that the molecules pass through a laser beam to ensure that effects of the evolution of the Doppler shift and of the optical intensity and phase at the position of the molecule are properly included. The results of this paper are compared to those of a deflection scheme [A. Marsman, D. Heinrich, M. Horbatsch, and E. A. Hessels, *Phys. Rev. A* **107**, 032811 (2023)] which uses  $\pi$  pulses to drive frequency-resolved transitions. This paper is part of an effort by the EDM<sup>3</sup> collaboration to measure the electric dipole moment of the electron using BaF molecules embedded in a cryogenic argon solid. Separation of BaF molecules will aid in producing a sufficiently pure solid.

DOI: [10.1103/PhysRevA.108.012811](https://doi.org/10.1103/PhysRevA.108.012811)

### I. INTRODUCTION

The bichromatic force uses two pairs of counterpropagating laser beams that are offset from each other in frequency. The frequency offset leads to beat notes in both directions, and, at the location of an atom or molecule, this beating leads to pulses (offset in time) arriving from each direction. The effect of these pulses is to cause a promotion to an excited state, followed by stimulated emission back down to the ground state. Bichromatic forces were first demonstrated by Grimm *et al.* [1]. As one quantum ( $\hbar\vec{k}$ ) of momentum is imparted to the atom or molecule for each excitation and each stimulated emission, strong forces are possible. For standard spontaneous-emission optical forces [2,3], the maximum force possible is  $\frac{1}{2}\hbar k/\tau$ , with the factor of 1/2 coming from equalized populations between the ground and excited states and  $\tau$  (the spontaneous-decay lifetime) being the average wait time between laser excitations. The bichromatic force allows for two quanta of momentum being imparted and allows for much shorter wait times.

Bichromatic forces have been used to manipulate atomic beams of Na [1,4], Rb [5–7], Cs [8], and metastable He [9–12] and Ar [13]. More recently, the use of bichromatic forces on molecules has become a topic of interest because of its distinct advantage of imparting many quanta of momentum in the average time interval between spontaneous-decay events. For molecules, where population can be lost due to branching ratios to other vibrational (or electronic) states, optical forces with fewer spontaneous decays require fewer repump lasers. Schemes for manipulating molecular beams with the

bichromatic force have been proposed for CaF [14,15], MgF [16,17], BaH [18], YbF [19], and  $^{137}\text{Ba}^{19}\text{F}$  [20]. Thus far, deflections have only been demonstrated using CaF [21] and SrOH [22].

In this paper, we calculate the deflection of a BaF beam due to the bichromatic force. The BaF molecule is being used by the EDM<sup>3</sup> collaboration to make an ultraprecise measurement [23] of the electric dipole moment of the electron. For the measurement, BaF molecules produced by a buffer-gas-cooled laser-ablation source are embedded in solid argon. It is necessary to separate the BaF molecules from the other ablation products via a deflection in order to produce an uncontaminated solid. For this purpose, a deflection of approximately 3 m/s (approximately 1000 quanta of photon momentum) is required. This deflection is much larger than demonstrated [21,22] deflections of other molecules using the bichromatic force.

In Sec. II we describe the density-matrix equations used to determine our deflections. Section III gives the results of our calculations and Sec. IV compares these results with the results of Ref. [24], which evaluates deflections caused by time-resolved  $\pi$  pulses driving frequency-resolved laser transitions.

### II. DENSITY-MATRIX CALCULATION

In this section we present a density-matrix calculation of BaF molecules being deflected [see Fig. 1(a)] by the bichromatic force. Since a BaF molecule in the  $A^2\Pi_{1/2}(v=0)$  state has a branching ratio [25] of 96.4% for decay to the  $X^2\Sigma_{1/2}(v=0)$  state, the 16 states of Fig. 1(b) form an almost closed system, and these 16 states are the only ones included in our density-matrix calculations. Because the ground state has more substates than the excited state, spontaneous decay

<sup>\*</sup>hessels@yorku.ca

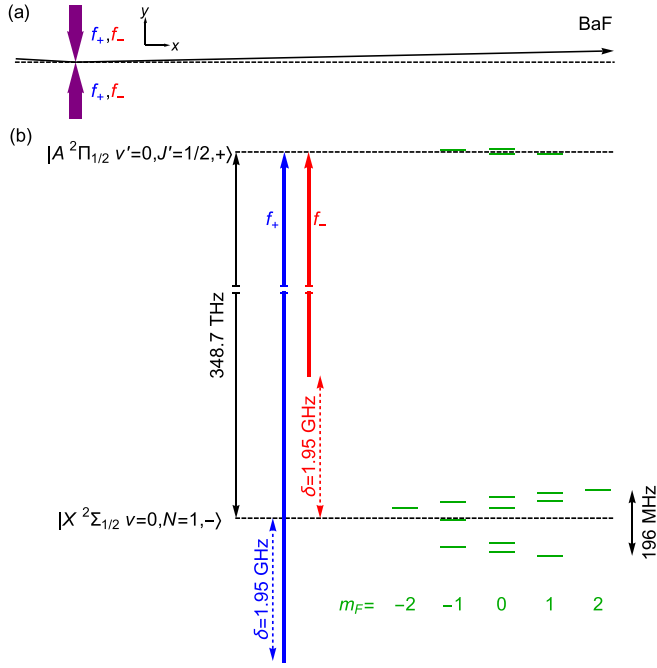


FIG. 1. The bichromatic force deflects a BaF molecule using two pairs of counterpropagating laser beams (a) that are linearly polarized in the  $\hat{z}$  direction and are offset from each other in frequency by  $\pm\delta$  (b). The structure of the  $X^2\Sigma_{1/2} v=0, N=1$  negative parity state and the  $A^2\Pi_{1/2} v'=0, j'=1/2$  positive parity state, shown at the right on an expanded scale in (b), is much smaller than  $\delta = 700/(2\pi\tau) = 1950$  MHz. A 20-G magnetic field (oriented  $60^\circ$  from  $\hat{z}$ ) lifts the degeneracy of the  $m_F$  levels and ensures that molecules do not remain in a dark state.

will result in the population quickly landing in a dark state (a linear combination of the ground states that is insensitive to laser excitation). To avoid this, the dark states are destabilized [26] by a magnetic field [27] which causes the molecules to Larmor precess into bright states. The magnetic field used is 20 G in the  $\hat{y}\sin(60^\circ) + \hat{z}\cos(60^\circ)$  direction of Fig. 1(a), but our results are found to be only mildly sensitive to the exact direction and magnitude of this field.

The time evolution of the density matrix elements is determined by numerically integrating their differential equations during the time period when the molecule passes through the laser beams. This time evolution is calculated in the zero-magnetic-field basis:

$$\begin{aligned} \frac{d\rho_{gg'}}{dt} &= i\omega_{g'g}\rho_{gg'} + i\sum_{g''}(\chi_{g''g'}\rho_{gg''} - \chi_{gg''}\rho_{g''g'}) \\ &\quad + \frac{i}{2}\sum_e(\Omega_{eg'}\rho_{ge} - \Omega_{ge}\rho_{eg'}) + \sum_{e,e'}\gamma_{ege'g'}\rho_{ee'}, \\ \frac{d\rho_{ee'}}{dt} &= i\omega_{e'e}\rho_{ee'} + i\sum_{e''}(\chi_{e''e'}\rho_{ee''} - \chi_{ee''}\rho_{e''e'}) \\ &\quad + \frac{i}{2}\sum_g(\Omega_{ge'}\rho_{eg} - \Omega_{eg}\rho_{ge'}) \\ &\quad - \frac{1}{2}\sum_{g,e''}(\gamma_{ege''g}\rho_{e''e'} + \gamma_{e''ge'g}\rho_{ee''). \end{aligned}$$

$$\begin{aligned} \frac{d\rho_{ge}}{dt} &= i(\omega_{eg} - \omega_0)\rho_{ge} + \frac{i}{2}\sum_{g'}\Omega_{g'e}\rho_{gg'} \\ &\quad + i\sum_{e'}\chi_{e'e}\rho_{ge'} - i\sum_{g'}\chi_{gg'}\rho_{g'e} \\ &\quad - \frac{i}{2}\sum_{e'}\Omega_{ge'}\rho_{e'e} - \frac{1}{2}\sum_{g',e'}\gamma_{e'g'eg'}\rho_{ge'}, \end{aligned} \quad (1)$$

where the indices  $g$  and  $e$  represent the 12 ground and four excited states, respectively. Here,  $\hbar\omega_{ab} = E_a - E_b$  is the zero-field energy difference between states  $|a\rangle$  and  $|b\rangle$ , with  $\hbar\chi_{ab} = -\langle a|\vec{\mu} \cdot \vec{B}|b\rangle$  being the elements of the Zeeman Hamiltonian. The energies and Zeeman elements are calculated using the methods detailed in the Appendix of Ref. [28] and are listed in Tables II and IV in the Appendix of this paper. The difference between the average energy of the  $|e\rangle$  states and the average of the  $|g\rangle$  states is denoted by  $\hbar\omega_0$ . Equation (1) uses the rotating-wave approximation to avoid the fast oscillations at the optical frequency  $\omega_0$ .

We use the complete formulation for spontaneous decay [29,30] which includes quantum-mechanical interference from the decay process using

$$\gamma_{ege'g'} = \frac{\omega^3}{3\pi\epsilon_0\hbar c^3} \vec{d}_{ge} \cdot \vec{d}_{e'g'}. \quad (2)$$

The diagonal elements  $\gamma_{egeg}$  are equal to the branching ratio times  $1/\tau$ . The off-diagonal elements properly account for quantum-mechanical interference and are included in calculations of the bichromatic force. For the present case, these terms lead to only small corrections.

The dipole matrix elements can be deduced from the measured lifetime of the  $A^2\Pi_{1/2}$  state ( $\tau = 57.1$  ns [31]), along with the branching ratio [25] between individual hyperfine states. These latter ratios are calculated using the methods described in Ref. [28]. The values of the electric dipole matrix elements are listed in Table III in the Appendix.

The Rabi frequencies in Eq. (1) are given by

$$\Omega_{eg}(t) = \frac{\vec{d}_{eg} \cdot \hat{z}E_0(x)}{\hbar} \sum_{s,\sigma=\pm 1} e^{i(sky + 2\pi\sigma\delta t - s\sigma\frac{\pi}{8} + \phi)} \Bigg|_{(x,y,z)=\vec{r}_m(t)}, \quad (3)$$

where the sum is over the four laser beams (with frequencies offset by  $\pm\delta$  and with  $\vec{k}$  in the  $\pm\hat{y}$  directions). For the present paper,  $\delta$  is chosen to be  $700/(2\pi\tau)$ , or 1950 MHz. Note our choice to express  $\delta$  as a frequency, rather than an angular frequency. The field amplitude  $E_0(x)$  includes the spatial profile of the laser beam, which is taken to be a top-hat shape (as, e.g., in Ref. [32]) approximated by a super-Gaussian function of the form

$$E_{\max}e^{-(x^2/w^2)^5}, \quad (4)$$

where the value of  $w$  is chosen to give an intensity profile with a full width at half maximum (FWHM) of 0.32 mm and  $E_{\max}$  is set to the value that gives the best approximation to  $\pi$  pulses for a multilevel system [15]:  $E_{\max} = 2\pi\delta\sqrt{6\pi\hbar\tau/(\lambda^3\epsilon_0)} = 1380$  V/cm (corresponding to a laser power of 2 W for each of the four beams).

Both the  $x$  dependence in the profile of Eq. (4) and the  $y$  found in the complex exponential of Eq. (3) are evaluated at the molecular position  $\vec{r}_m(t)$ . The trajectory of the molecule is obtained from its original position, its initial velocity (assumed to be 150 m/s—a typical speed for a BaF molecule in a 4-K helium-buffer-gas-cooled beam [33]), and the force obtained [34] from Ehrenfest’s theorem:

$$\vec{F}(t) = -\hbar \sum_{e,g} \text{Re}[\rho_{eg}(t) \nabla \Omega_{ge}(\vec{r}, t)] \Big|_{\vec{r}=\vec{r}_m(t)}. \quad (5)$$

As discussed above, the density-matrix treatment is not complete in that the 16 levels do not quite form a closed system. The remaining branching ratio (3.6%) causes population to be lost out of the cycling transition and is primarily due to radiative decay down to the  $X^2\Sigma_{1/2}(v=1)$  state (3.5%) [25], with much smaller contributions for decays to the  $X^2\Sigma_{1/2}(v>1)$  states and the  $A'^2\Delta_{3/2}$  state. Spontaneous decay to the latter state causes the molecule to change its parity upon its second decay down to the  $X^2\Sigma_{1/2}$  state. The net effect is that every spontaneous emission leads to 3.6% of the excited-state population going into a dark state that will no longer experience the bichromatic force. Fortunately, as we will see, the bichromatic force can be applied with very little spontaneous emission occurring, and therefore this loss remains relatively small and no repumping into the cycling states is required.

We treat these dark states by reducing the population of the 16 states in accordance with the buildup of population into the dark states. Our density-matrix calculation continues with only the remaining population present, and therefore our results apply only to the molecules that are not lost to the dark state. Although it is tempting to treat the dark state population by including an additional state in our density-matrix equations, this strategy is incompatible with our strategy of treating the force [Eq. (2)] and the molecular trajectory classically. The inconsistency results from the fact that the dark state no longer feels a force. The full quantum description, as seen in atom interferometry, would include both the momentum and the internal state of the molecule and would allow each component associated with an internal state (e.g., the dark state component) to have a different momentum. We avoid this complication by ignoring the dark state during our calculation, the effect of which is to correctly calculate the force on those molecules that do not decay to the dark state. However, to properly account for the dark state, we postprocess our data to determine the fraction of the population that would decay to the dark state during each time bin  $dt$  (by multiplying the adjusted excited-state population by  $dt$  times 3.6%) and incrementing the dark-state population (and decrementing the excited-state population by this fraction).

The density-matrix elements, along with the components of  $\vec{r}_m(t)$  and  $\vec{v}_m(t)$ , are numerically integrated over the  $\approx 2.7 \mu\text{s}$  that it takes for the molecules to pass through the laser profile. These integrations are computationally intensive given the 3.9-GHz frequency difference between the two laser beams, which leads to fast oscillations in the density-matrix elements, and these oscillations must be calculated accurately. The integration is performed using a suite of custom-written C++ programs. These are compiled and run on the

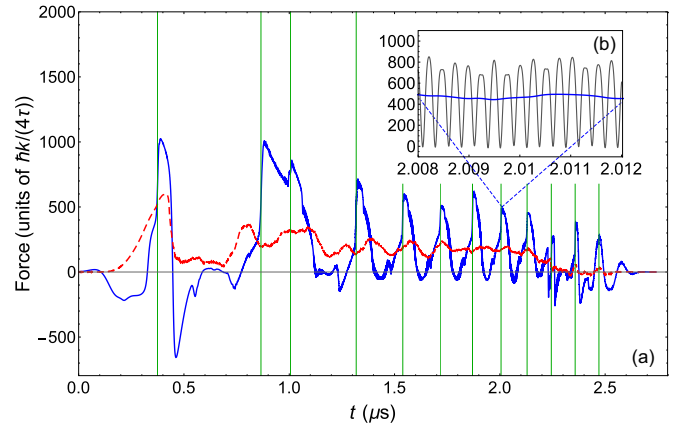


FIG. 2. The bichromatic force on the BaF molecule (with initial velocity of  $v_y^{\text{init}} = -1$  m/s) as it passes through the bichromatic laser beams. (b) The force oscillates at the beat frequency (of  $2 \times 1950$  MHz). (a) The force averaged over these fast oscillations. The blue solid curve is the force for a molecule initially on axis, and the peaks vs time occur each time the molecule moves by one half of a wavelength ( $\lambda/2$ ), where the fields of the two beams interfere constructively (the times at which the molecule is at these positions are indicated by green vertical lines). The red dashed curve is the force averaged over initial position ( $0 \leq y^{\text{init}} < \lambda/2$ ). A large average force of over  $200\hbar k/(4\tau)$  is calculated.

high-performance cluster of the Digital Research Alliance of Canada and use the GNU scientific library for the numerical integration. An adaptive Runge-Kutta-Fehlberg integration method is employed with absolute and relative tolerances set at  $10^{-6}$ .

### III. RESULTS

We start by considering a molecule that is initially at  $y^{\text{init}} = 0$  (on axis, see Fig. 1) with a small downward velocity of  $v_y^{\text{init}} = -1$  m/s. The force on the BaF molecule as it traverses the bichromatic laser beams is determined from our numerical integration and is shown in Fig. 2. The inset in the figure shows that the force oscillates at the beat frequency ( $2 \times 1950$  MHz), and the forces shown in Fig. 2(a) are the averages over these fast oscillations. The blue solid curve shows the force versus time for initial conditions  $v_y^{\text{init}} = -1$  and  $y^{\text{init}} = 0$ . The force has a peak value each time the molecule is displaced by a half wavelength, showing that there is a strong dependence on the relative phases of the upward and downward directed beams. The force is large when the fields are interfering constructively, and small when they are interfering destructively. Because of this dependence, the force also depends strongly on  $y^{\text{init}}$  as this value is varied over half of the laser wavelength,  $\lambda$ . Since our molecular beam has a much larger extent than  $\lambda$  along  $y$ , we average the force over this initial position (averaging over  $y^{\text{init}}$  values that span  $\lambda/2$ ), as shown by the red dashed curve in Fig. 2.

Note that the averaged calculated force is more than 200 times larger than the spontaneous-emission optical force of  $\frac{1}{4}\hbar k/\tau$ , where here the usual factor of 1/2 for a two-level system is replaced by 1/4 since now only one quarter of our 16 states are excited states. This force can be compared to

a simplified model for the bichromatic force in a two-level system, in which the laser fields act as a series of  $\pi$  pulses, with each period  $T = 1/(2\delta)$  of the beat frequency having one pulse from the upward-directed laser followed a time  $T/4$  later by a pulse from the downward-directed laser. Ideally, the first pulse causes a laser excitation and the second causes a stimulated emission back to the ground state, leading to a force of  $2\hbar k/T$ . However, a spontaneous emission (if it occurs in the time interval between the first and second pulse) can reverse this sequence, leading to a force of  $-2\hbar k/T$ . Fortunately, another spontaneous emission (if it occurs in the  $3T/4$  interval after the second pulse) again reverses the force, and since this time interval is three times larger it is more likely to occur. As a result, this simple model predicts a force of  $\frac{3}{4}2\hbar k/T - \frac{1}{4}2\hbar k/T = \hbar k/T$ . This estimate is approximately a factor of 4 larger than our calculated average force of  $200\frac{1}{4}\hbar k/\tau = 0.23\hbar k/T$ . Part of this factor of 4 results from the reduced effectiveness of the bichromatic force for a multilevel system such as the one shown in Fig. 1(b).

The first reason for reduced effectiveness is that the number of substates of the ground state is larger than that of the excited state (the excited states represent one fourth rather than one half of the states), which reduces the fraction of molecules that can participate at any time. Second, as discussed above, dark states would make the molecules insensitive to the lasers, reducing the force to zero. The application of a magnetic field avoids the zeroing of the force, but a reduction is still seen. Finally, because each  $g$  state has a different dipole matrix element connecting it to the excited states (and, to a smaller extent, because each has a different resonant frequency) it is not possible to perfectly meet the  $\pi$ -pulse condition for all of the ground substates.

These factors, along with effects that are already present in the two-level system (such as the interference between the fields from the two directions), account for the factor of 4 reduction in force compared to the simple model. This factor is similar to the reduction calculated in other works [15,22].

Figure 3 shows the time progression of the total excited-state and dark state populations for  $v_y^{\text{init}} = -1$  m/s. Note that the population in the dark state builds up to approximately 23% by the time the molecules have passed through the beam, allowing the majority of the molecules to experience the full deflection force of Fig. 2.

The population in the excited state is approximately 15% on average during the time the molecules spend in the laser beams. The integral of this fraction over the time that it takes to pass through the 0.32-mm laser beams implies that there are only approximately six spontaneous emission events per molecule, whereas the molecule has received approximately 1600 quanta ( $1600\hbar k$ ) of momentum kicks from the lasers.

The inset in Fig. 3 shows that the excited-state population oscillates at the 3.9-GHz beat frequency, as the population is excited by one laser followed by stimulated emission from the oppositely directed laser beam. The figure shows the excited-state population for  $y^{\text{init}} = 0$  (blue), as well as the result averaged over  $y^{\text{init}}$  (red dashed).

Results for different  $v_y^{\text{init}}$  are illustrated in Fig. 4, where the transverse velocity ( $v_y$ ) is plotted versus time for

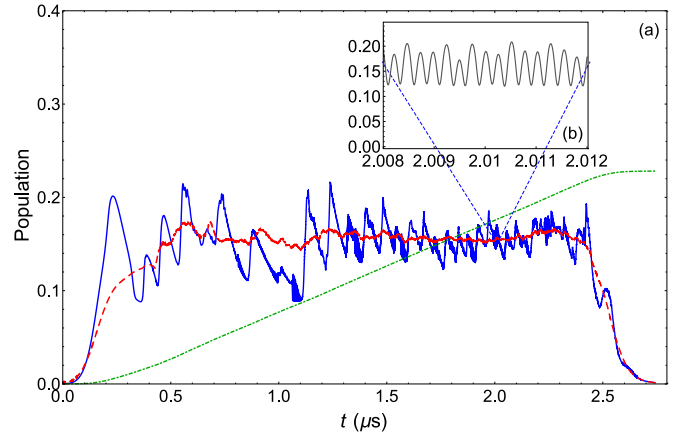


FIG. 3. The total populations of the excited and dark states for  $v_y^{\text{init}} = -1$  m/s. Approximately 15% of the molecules are in the excited state (blue) during the time that they pass through the laser beam. (b) This population oscillates at the 3.9-GHz beat frequency, as the population is excited up followed by stimulated emission back to the ground state. (a) A time-averaged view that averages over these oscillations. The blue solid line is for  $y^{\text{init}} = 0$  and the red dashed curve is averaged over  $y^{\text{init}}$ . The population of the dark state (green dash-dot) steadily increases to approximately 23% as the molecules pass through the laser, allowing the remaining 77% of the molecules to experience the full force shown in Fig. 2.

$v_y^{\text{init}} = -1, -2, -3,$  and  $-4$  m/s. These curves depend on  $y^{\text{init}}$ , and the figure shows the averages over  $y^{\text{init}}$ , as well as the one-standard-deviation range for variations from this average value. In each case, a deflection of approximately 5 m/s changes the transverse velocity into the positive direction.

For the present paper, the deflection is only needed for the small range of  $v_y^{\text{init}}$  shown in Fig. 4, but Fig. 5 shows that large deflections persist for a wide range of initial transverse velocities. Again an average over a half wavelength for  $y^{\text{init}}$  is used for this figure. As expected, the large value of  $\delta$  leads to a large force over a wide range of transverse velocities.

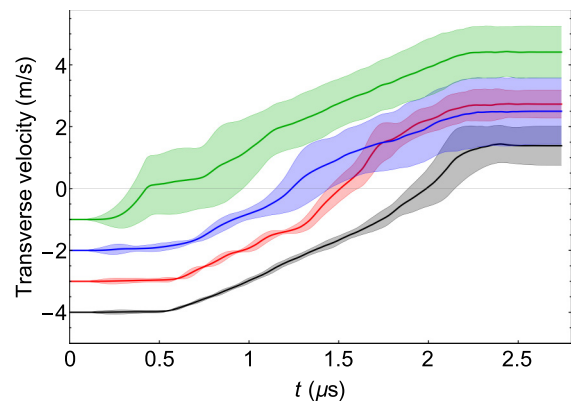


FIG. 4. The transverse velocity ( $v_y$ ) vs time (while passing through the bichromatic laser beams) for BaF molecules starting with  $v_x = 150$  m/s and  $v_y^{\text{init}} = -4, -3, -2,$  and  $-1$  m/s. The molecules are deflected upward by approximately 5 m/s.

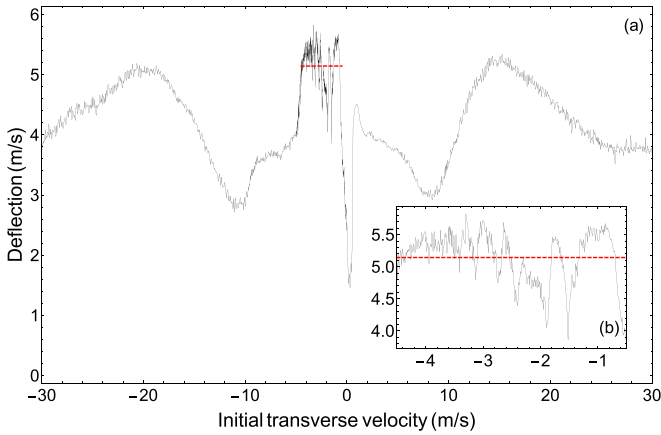


FIG. 5. The deflection of a BaF beam (with a longitudinal speed  $v_x = 150$  m/s) after passing through the bichromatic laser beams as a function of its initial transverse velocity ( $v_y$ ). Note that large deflections occur over a wide range of initial  $v_y$ . For the present paper, we focus on initial transverse velocities in the range of  $-4.5$  to  $-0.5$  m/s (inset), where the average deflection is 5.1 m/s (red dashed line).

#### IV. COMPARISON TO THE DEFLECTION SCHEME USING TIME-RESOLVED $\pi$ PULSES

The results of the present paper can be compared to a recent work [24] which calculated deflections of BaF molecules caused by short-duration  $\pi$  pulses in a large magnetic field which resolved individual laser transitions. Table I compares the parameters and results of that work to the present paper. The time-resolved  $\pi$  pulses and frequency-resolved laser transitions in Ref. [24] had the advantages of (i) avoiding interference between the fields from the oppositely directed lasers, (ii) being able to tune the individual laser powers to meet the  $\pi$ -pulse condition for each ground state, and (iii) being able to adjust the timing to maximize the net force. These advantages can be seen in the third row of Table I, where Ref. [24] has a 50% larger momentum imparted per

period (per 10-ns period for the pair of  $\pi$  pulses in Ref. [24] and per period of the beat note in this paper). In both works, the power (at each frequency) per laser beam is approximately 2 W. However, the extent of the laser beam in the present paper is 0.32 mm in the  $z$  direction [see Fig. 1(a)], whereas in Ref. [24] the extent was 1 mm, which allowed for interaction with three times the number of BaF molecules.

To make a more direct comparison to the previous work [24], we also calculated bichromatic deflections with a 2-W laser beam that has a FWHM of 1 mm in the  $z$  direction, and these results are shown in column 4 of Table I. The results in this column show that the bichromatic force is, in most respects, a better choice for deflection compared to the  $\pi$ -pulse scheme. The main advantage comes from the rate at which pairs of laser pulses are incident on the molecules, which is more than a factor of 20 faster (see row 2) for the bichromatic case. Even with the lower efficiency per period, the net force (see row 1) is still more than an order of magnitude larger. More importantly, the smaller period allows for more momentum transfer in the average time interval between spontaneous-emission events (see row 10). For both columns 3 and 4, spontaneous emission is rare enough that less than 25% of the population is lost to a dark state, and therefore no repump lasers are needed.

In principle, the  $\pi$ -pulse scheme could also eliminate the need for repump lasers by having a much faster rate of  $\pi$  pulses, but this would considerably complicate the scheme since the shorter pulses would require higher laser power, as well as a larger magnetic field to resolve the individual transitions (as discussed in Ref. [24]).

One way in which the  $\pi$ -pulse scheme is superior is in the robustness of the force. In Ref. [24], the deflection is found to vary by only 2% when the electric field of each of the laser beams is randomly varied between 0.95 and 1.05 of their nominal values. Here, by comparison (as shown in row 12 of Table I), the deflection varies by 16% when the relative amplitudes (electric fields) for the four lasers are randomly varied in the more limited range of 0.99 to 1.01. For Ref. [24],

TABLE I. A comparison of the parameters and results of this paper to those of Ref. [24].

Quantity	Units	Bichromatic: this paper	Bichromatic: expanded beam	$\pi$ pulses: Ref. [24]
Momentum change, $\Delta p_y$ , per lifetime	$\hbar k$	50	27	2
Period (beat period or cycle period)	ns	0.26	0.45	10
Momentum change, $\Delta p_y$ , per period	$\hbar k$	0.23	0.21	0.35
Number of frequencies: Main laser		2	2	6
Number of frequencies: Repump laser		0	0	6
Power per beam at each frequency	W	2	2	$\approx 2$
Laser field $E_0$ per beam at each frequency	V/cm	1380	780	$\approx 200$
Laser intensity FWHM: $z$ direction of Fig. 1(a)	mm	0.32	1	1
Laser intensity FWHM: $x$ direction of Fig. 1(a)	mm	0.32	0.32	5
Momentum change, $\Delta p_y$ , per spontaneous decay	$\hbar k$	270	140	20
Applied magnetic field	G	20	20	1000
Change in $\Delta v_y$ for imperfect laser parameters				
$E_0$ for each laser varied by the factor specified		[0.99–1.01]: 10%	15%	[0.95–1.05]: 2%
Relative phases varied by the angle range specified		[0–25 mrad]: 10%	16%	[0– $2\pi$ ]: 6%
Each laser includes 0–1% of other polarization		[0–1%]: 6%	5%	[0–1%]: 1%
Deflection, $\Delta v_y$	m/s	5.1	2.7	2.6

TABLE II. The energies of the ground states and excited states in zero magnetic field.

State	$F$	$m_F$	$E/h$ (MHz)
g1	1	-1	-94.947
g2	1	0	-94.947
g3	1	+1	-94.947
g4	0	0	-67.134
g5	1	-1	22.715
g6	1	0	22.715
g7	1	+1	22.715
g8	2	-2	56.766
g9	2	-1	56.766
g10	2	0	56.766
g11	2	+1	56.766
g12	2	+2	56.766
e1	1	-1	$\omega_0/(2\pi) - 1.25$
e2	1	0	$\omega_0/(2\pi) - 1.25$
e3	1	+1	$\omega_0/(2\pi) - 1.25$
e4	0	0	$\omega_0/(2\pi) + 3.75$

TABLE III. The electric dipole matrix elements between the states of Table II.

Ground state	Excited state	Polarization	$d_{eg}$ ( $ea_0$ )
g1	e1	0	-1.17
g1	e2	+1	1.17
g1	e4	+1	0.839
g2	e1	-1	1.17
g2	e3	+1	1.17
g2	e4	0	-0.839
g3	e2	-1	-1.17
g3	e3	0	-1.17
g3	e4	-1	0.839
g4	e1	-1	1.105
g4	e2	0	-1.105
g4	e3	+1	-1.105
g5	e1	0	-0.063
g5	e2	+1	0.063
g5	e4	+1	-1.062
g6	e1	-1	-0.063
g6	e3	+1	-0.063
g6	e4	0	-1.062
g7	e2	-1	-0.063
g7	e3	0	-0.063
g7	e4	-1	-1.062
g8	e1	+1	-0.957
g9	e1	0	0.677
g9	e2	+1	0.677
g10	e1	-1	-0.391
g10	e2	0	-0.781
g10	e3	+1	0.391
g11	e2	-1	0.677
g11	e3	0	-0.677
g12	e3	-1	-0.957

TABLE IV. The nonzero magnetic dipole matrix elements between the states of Table II (in spherical tensor form).

State 1	State 2	Component, $q$	$\langle 1 \mu_q 2\rangle(\mu_B)$
g1	g1	0	0.498764
g1	g2	-1	-0.508397
g2	g3	-1	-0.508397
g3	g3	0	-0.498765
g4	g1	1	0.0611559
g4	g2	0	-0.0540664
g4	g3	-1	0.0611559
g5	g1	0	0.0861576
g5	g2	-1	-0.0838738
g5	g4	-1	1.00933
g5	g5	0	-0.976845
g6	g1	1	-0.0838738
g6	g3	-1	0.0838738
g6	g4	0	-1.00037
g6	g5	1	0.986477
g7	g2	1	0.0838738
g7	g3	0	-0.0861576
g7	g4	1	1.00933
g7	g6	1	0.986477
g7	g7	0	0.976845
g8	g1	-1	-1.23099
g8	g5	-1	-0.0572771
g8	g8	0	-0.97496
g9	g1	0	-0.864044
g9	g2	-1	-0.87044
g9	g5	0	-0.0390138
g9	g6	-1	0.040501
g9	g8	1	-0.69732
g9	g9	0	-0.48748
g10	g1	1	-0.502549
g10	g2	0	-0.997712
g10	g3	-1	-0.502549
g10	g5	1	-0.0233833
g10	g6	0	0.0450493
g10	g7	-1	-0.0233833
g10	g9	1	-0.85404
g11	g10	1	-0.85404
g11	g11	0	0.48748
g11	g2	1	-0.87044
g11	g3	0	-0.864044
g11	g6	1	0.040501
g11	g7	0	-0.0390138
g12	g11	1	0.69732
g12	g12	0	0.97496
g12	g3	1	1.23099
g12	g7	1	0.0572771
e1	e1	0	0.20784
e3	e3	0	-0.20784
e4	e2	0	-0.20784

variation of the relative phase of the laser beam (randomly selected over the full range of 0 to  $2\pi$ ) led to a variation in the deflection of 6%. For the bichromatic force, the relative phases need to be fixed to get a net force, and we find that varying the relative phases randomly within the range of 0 to 0.025 rad leads to a variation in deflection of 15%. Finally, in

Ref. [24] having imperfect polarization (i.e., an admixture of the opposite circular polarization) randomly picked between 0 and 1% led to a variation in deflection of 1%. Here, a similar level of imperfect polarization (with an admixture of polarization along the orthogonal  $\hat{x}$  direction) leads to a variation in deflection of 5%.

The final row of Table I shows that the deflection from the laser beams of Ref. [24] is nearly equal to that from the bichromatic laser beams (column 4). Although the bichromatic deflection scheme does require better control of the laser parameters, it is still far simpler to implement in that it only requires two (compared to 12) laser frequencies and it requires a much smaller magnetic field.

## V. CONCLUSIONS

In this paper, we have performed a complete density-matrix simulation of deflections of BaF molecules using the bichromatic force. This deflection would allow for a beam of  $^{138}\text{Ba}^{19}\text{F}$  to be separated from other laser ablation products coming from a buffer-gas-cooled laser-ablation source, as required by the EDM<sup>3</sup> collaboration for their planned

measurement of the electric dipole moment of the electron using BaF molecules embedded in an Ar solid.

## ACKNOWLEDGMENTS

We acknowledge support from the Gordon and Betty Moore Foundation, the Alfred P. Sloan Foundation, the John Templeton Foundation (through the Center for Fundamental Physics at Northwestern University), the Natural Sciences and Engineering Research Council of Canada, the Canada Foundation for Innovation, the Ontario Research Fund, and York University. Computations for this paper were enabled by support provided by the Digital Research Alliance of Canada, Compute Ontario, and SHARCNET.

## APPENDIX

The energies, Zeeman structure, and dipole matrix elements for our system were calculated using the methods described in Ref. [28]. The energies (in zero magnetic field) are shown in Table II, the dipole matrix elements are shown in Table III, and the Zeeman matrix elements are shown in Table IV.

- 
- [1] R. Grimm, Y. B. Ovchinnikov, A. I. Sidorov, and V. S. Letokhov, Observation of a Strong Rectified Dipole Force in a Bichromatic Standing Light Wave, *Phys. Rev. Lett.* **65**, 1415 (1990).
  - [2] A. Ashkin, Acceleration and Trapping of Particles by Radiation Pressure, *Phys. Rev. Lett.* **24**, 156 (1970).
  - [3] R. Schieder, H. Walther, and L. Wöste, Atomic beam deflection by the light of a tunable dye laser, *Opt. Commun.* **5**, 337 (1972).
  - [4] Y. B. Ovchinnikov, R. Grimm, A. I. Sidorov, and V. S. Letokhov, Rectified dipole force in a bichromatic standing light wave, *Opt. Commun.* **102**, 155 (1993).
  - [5] R. Gupta, C. Xie, S. Padua, H. Batelaan, and H. Metcalf, Bichromatic Laser Cooling in a Three-Level System, *Phys. Rev. Lett.* **71**, 3087 (1993).
  - [6] M. R. Williams, F. Chi, M. T. Cashen, and H. Metcalf, Measurement of the bichromatic optical force on Rb atoms, *Phys. Rev. A* **60**, R1763 (1999).
  - [7] M. R. Williams, F. Chi, M. T. Cashen, and H. Metcalf, Bichromatic force measurements using atomic beam deflections, *Phys. Rev. A* **61**, 023408 (2000).
  - [8] J. Söding, R. Grimm, Y. B. Ovchinnikov, P. Bouyer, and C. Salomon, Short-Distance Atomic Beam Deceleration with a Stimulated Light Force, *Phys. Rev. Lett.* **78**, 1420 (1997).
  - [9] M. Cashen, O. Rivoire, V. Romanenko, L. Yatsenko, and H. Metcalf, Strong optical forces in frequency-modulated light, *Phys. Rev. A* **64**, 063411 (2001).
  - [10] M. Partlow, X. Miao, J. Bochmann, M. Cashen, and H. Metcalf, Bichromatic Slowing and Collimation to Make an Intense Helium Beam, *Phys. Rev. Lett.* **93**, 213004 (2004).
  - [11] M. A. Chieda and E. E. Eyler, Bichromatic slowing of metastable helium, *Phys. Rev. A* **86**, 053415 (2012).
  - [12] C. Corder, B. Arnold, and H. Metcalf, Laser Cooling without Spontaneous Emission, *Phys. Rev. Lett.* **114**, 043002 (2015).
  - [13] Z. Feng, S. Ebser, L. Ringena, F. Ritterbusch, and M. K. Oberthaler, Bichromatic force on metastable argon for atom-trap trace analysis, *Phys. Rev. A* **96**, 013424 (2017).
  - [14] M. A. Chieda and E. E. Eyler, Prospects for rapid deceleration of small molecules by optical bichromatic forces, *Phys. Rev. A* **84**, 063401 (2011).
  - [15] L. Aldridge, S. E. Galica, and E. E. Eyler, Simulations of the bichromatic force in multilevel systems, *Phys. Rev. A* **93**, 013419 (2016).
  - [16] X. Yang, C. Li, Y. Yin, S. Xu, X. Li, Y. Xia, and J. Yin, Bichromatic slowing of MGF molecules in multilevel systems, *J. Phys. B* **50**, 015001 (2017).
  - [17] D. Dai, Y. Xia, Y. Fang, L. Xu, Y. Yin, X. Li, X. Yang, and J. Yin, Efficient stimulated slowing and cooling of the magnesium fluoride molecular beam, *J. Phys. B* **48**, 085302 (2015).
  - [18] K. Wenz, I. Kozyryev, R. L. McNally, L. Aldridge, and T. Zelevinsky, Large molasses-like cooling forces for molecules using polychromatic optical fields: A theoretical description, *Phys. Rev. Res.* **2**, 043377 (2020).
  - [19] Y. Yin, S. Xu, M. Xia, Y. Xia, and J. Yin, Optically stimulated slowing of polar heavy-atom molecules with a constant beat phase, *Phys. Rev. A* **97**, 043403 (2018).
  - [20] F. Kogel, M. Rockenhäuser, R. Albrecht, and T. Langen, A laser cooling scheme for precision measurements using fermionic barium monofluoride ( $^{137}\text{Ba}^{19}\text{F}$ ) molecules, *New J. Phys.* **23**, 095003 (2021).
  - [21] S. E. Galica, L. Aldridge, D. J. McCarron, E. E. Eyler, and P. L. Gould, Deflection of a molecular beam using the bichromatic stimulated force, *Phys. Rev. A* **98**, 023408 (2018).
  - [22] I. Kozyryev, L. Baum, L. Aldridge, P. Yu, E. E. Eyler, and J. M. Doyle, Coherent Bichromatic Force Deflection of Molecules, *Phys. Rev. Lett.* **120**, 063205 (2018).
  - [23] A. C. Vutha, M. Horbatsch, and E. A. Hessels, Orientation-dependent hyperfine structure of polar molecules in a rare-gas

- matrix: A scheme for measuring the electron electric dipole moment, *Phys. Rev. A* **98**, 032513 (2018).
- [24] A. Marsman, D. Heinrich, M. Horbatsch, and E. A. Hessels, Large optical forces on a barium monofluoride molecule using laser pulses for stimulated absorption and emission: A full density-matrix simulation, *Phys. Rev. A* **107**, 032811 (2023).
- [25] Y. Hao, L. F. Pašteka, L. Visscher, P. Aggarwal, H. L. Bethlem, A. Boeschoten, A. Borschevsky, M. Denis, K. Esajas, S. Hoekstra, and K. Jungmann, High accuracy theoretical investigations of CaF, SrF, and BaF and implications for laser-cooling, *J. Chem. Phys.* **151**, 034302 (2019).
- [26] D. J. Berkeland and M. G. Boshier, Destabilization of dark states and optical spectroscopy in Zeeman-degenerate atomic systems, *Phys. Rev. A* **65**, 033413 (2002).
- [27] E. S. Shuman, J. F. Barry, and D. DeMille, Laser cooling of a diatomic molecule, *Nature (London)* **467**, 820 (2010).
- [28] P. Kaebert, M. Stepanova, T. Poll, M. Petzold, S. Xu, M. Siercke, and S. Ospelkaus, Characterizing the Zeeman slowing force for  $^{40}\text{Ca } ^{19}\text{F}$  molecules, *New J. Phys.* **23**, 093013 (2021).
- [29] D. A. Cardimona and C. R. Stroud, Jr., Spontaneous radiative coupling of atomic energy levels, *Phys. Rev. A* **27**, 2456 (1983).
- [30] A. Marsman, M. Horbatsch, and E. A. Hessels, Shifts due to distant neighboring resonances for laser measurements of  $2 \ ^3S_1$ -to- $2 \ ^3P_j$  transitions of helium, *Phys. Rev. A* **86**, 040501(R) (2012).
- [31] P. Aggarwal, V. R. Marshall, H. L. Bethlem, A. Boeschoten, A. Borschevsky, M. Denis, K. Esajas, Y. Hao, S. Hoekstra, K. Jungmann, T. B. Meijknecht, M. C. Mooij, R. G. E. Timmermans, A. Touwen, W. Ubachs, S. M. Vermeulen, L. Willmann, Y. Yin, and A. Zapara, Lifetime measurements of the  $A^2\Pi_{1/2}$  and  $A^2\Pi_{3/2}$  states in BaF, *Phys. Rev. A* **100**, 052503 (2019).
- [32] H. Ma, Z. Liu, P. Jiang, X. Xu, and S. Du, Improvement of Galilean refractive beam shaping system for accurately generating near-diffraction-limited flattop beam with arbitrary beam size, *Opt. Express* **19**, 13105 (2011).
- [33] S. Truppe, M. Hambach, S. M. Skoff, N. E. Bulleid, J. S. Bumby, R. J. Hendricks, E. A. Hinds, B. E. Sauer, and M. R. Tarbutt, A buffer gas beam source for short, intense and slow molecular pulses, *J. Mod. Opt.* **65**, 648 (2018).
- [34] R. J. Cook, Atomic motion in resonant radiation: An application of Ehrenfest's theorem, *Phys. Rev. A* **20**, 224 (1979).